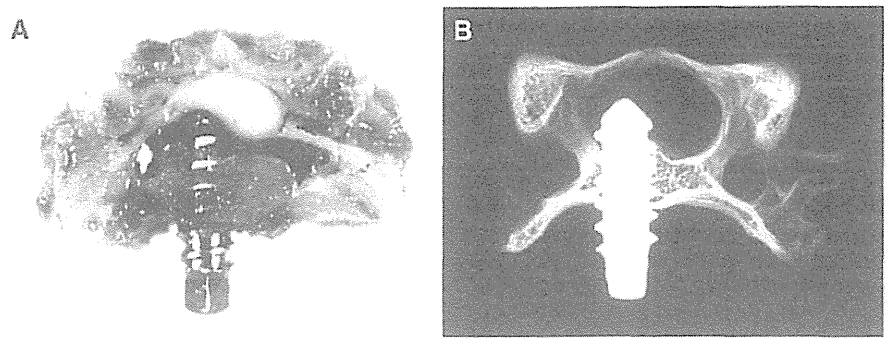

Fig. 8.1 (a) Transverse slab of the C5 vertebra and the spinal cord with the screw cut 3 mm in thickness, showing the deformation of the spinal cord by the unilateral compression. (b) Softex radiograph showing the position of the screw and the extent of compression

8.2.2 *Tissue Preparation and Staining*

Rabbits were sacrificed by the intravenous injection of a high dose of pentobarbiturate 1 week after the surgery for hematoxylin and eosins (HE), Kluver-Barrera (KB) medullary sheath staining, and GFAP immunohistostaining and 48 h after the surgery for RCA-1 immunohistostaining. The cervical spine and spinal cord were removed together with the screw in situ. The specimen was fixed in 10 % neutral-buffered formalin. The C5 vertebra was transversely cut above and below the screw with a diamond band saw to obtain a 3-mm-thick slab (Fig. 8.1a). A Softex radiograph of the slab was taken for the assessment of the position of the screw (Fig. 8.1b). The screw was then removed from the slab. Spinal cord specimens were taken out of the slabs and fixed in the same fixative, and sections 5 μm thick were obtained. The sections were stained by HE and KB medullary sheath staining for the observation of the axons and myelins and for the measurement of the area.

8.2.3 *Measurement of Compression Rate*

On the Softex radiographs of the transverse slabs of the C5 vertebrae with the screws, the areas of the protruding screws in the spinal canal and the areas of the spinal canals were measured using an image scanner and a personal computer with the software of the NIH image version 1.6. The ratio of the former to the latter was defined as "the compression rate."

8.2.4 *Measurement of Gray and White Matter Area in Each Half of the Spinal Cord*

On the slide of the KB medullary sheath staining, the spinal cord was divided into the compressed half and the contralateral half by the line of anterior median fissure and the posterior median sulcus through the central canal. The areas of the gray and white matter in each half of the spinal cord were measured using the image scanner interfaced with a computer.

8.2.5 *Immunohistochemistry*

Immunohistostaining of the astrocyte was carried out using an antibody to GFAP (polyclonal antibody; Dako, Glostrup, Denmark). Microglia were stained with an immunoperoxidase method using a lectin Ricinus communis agglutinin (RCA-1; Vector Laboratories, Burlingame, CA, USA) according to the method described by He and colleagues [13].

8.2.6 *Count of Glial Cells*

To count the GFAP-positive astrocytes, ten selected sections of the anterior and dorsal horns in the gray matter and the anterior, lateral, and dorsal funiculi in the white matter on the compressed and contralateral halves were determined on the GFAP staining slide; the center of each anterior and posterior horn section was defined as the midpoint of the line between the central canal and the tip of the anterior and dorsal horns. The center of each funiculus section was defined as the midpoint of the thickness of the funiculus. The section covered an area measuring 0.21×0.32 mm. The density of GFAP-positive astrocytes was calculated from the number of the cells in each section. The density of GFAP-positive astrocytes in the gray matter was defined as the average of the densities in the anterior and dorsal horns. The density of GFAP-positive astrocytes in the white matter was defined as the average of the densities in the anterior, lateral, and dorsal funiculi.

8.3 Results

The compression rate was defined by the ratio of the area of the protruding screw in the spinal canal to the area of the spinal canal. The compression rate was 17.1 ± 3.7 % (mean $\pm$ SD) in the mild compression group and 31.8 ± 3.2 % in the moderate compression group. The difference in the rate between the mild compression and moderate compression was considered extremely significant by unpaired t-test ($p < 0.0001$).

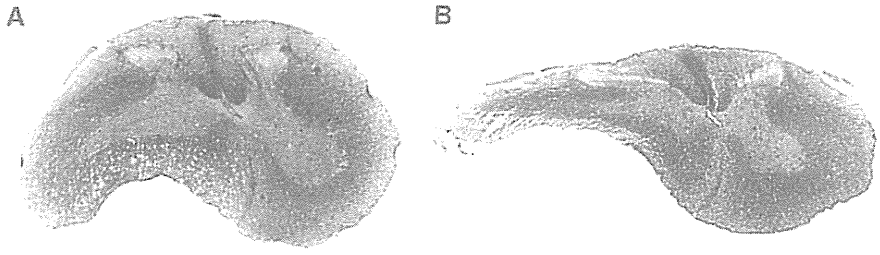

Fig. 8.2 The spinal cord was deformed into the shape of a reversed comma. The compressed half of the spinal cord was shaped like a boomerang and the contralateral half like a semicircle. The midline of the spinal cord, connecting the anterior median fissure to the posterior median sulcus through the central canal, was curved convexly to the contralateral half. (**a**) Under mild compression and (**b**) under moderate compression (Kluver-Barrera, ×10)

No apparent abnormal walking or movements of the upper and lower limbs were observed during the observation period of 1 week after surgery in rabbit (Tarlov rate 4).

8.3.1 Morphologic Change

In these animals, the spinal cord was deformed into the shape of a reversed comma. The compressed half of the spinal cord was shaped like a boomerang and the contralateral half like a semicircle. The midline of the spinal cord, connecting the anterior median fissure to the posterior median sulcus through the central canal, was curved convexly to the contralateral half. The anterior funiculus and the anterior horn were flattened in the compressed half (Fig. 8.2).

8.3.2 Area of Gray Matter and White Matter in Compressed Half and Contralateral Half

The area of each half of the spinal cord is shown in Table 8.1. The areas of both halves with moderate compression were significantly smaller than those in the sham animals ($p<0.001$), as were those associated with mild compression ($p<0.01$). Comparisons between the compressed and contralateral halves revealed no significant differences in surface areas following mild compression, whereas there were significant differences with moderate compression ($p<0.05$).

To analyze the reductions in the gray vs. white matter, the ratio of the gray matter to the white matter (gray/white matter) was calculated. However, via this approach, no significant differences in the ratios between the compressed and contralateral halves were found.

Table 8.1 Area and ratio of the gray matter to the white matter area (gray/white matter) under the compression (mean ± SEM)

	Compressed half		Contralateral half	
	Area	Gray/white matter	Area	Gray/white matter
Sham[a]	5.89±0.17	0.30±0.02		
Mild compression	5.06±0.22	0.27±0.02	5.29±0.21	0.25±0.01
Moderate compression	3.75±0.31[b, c, e]	0.23±0.03	4.32±0.24[b, d]	0.24±0.01

[a]Average of both halves of the spinal cord
[b]Significantly lower than sham ($p<0.001$)
[c]Significantly lower than the compressed half in mild compression ($p<0.001$)
[d]Significantly lower than the contralateral half in mild compression ($p<0.01$)
[e]Significantly lower than the contralateral half in moderate compression ($p<0.05$)

8.3.3 *Astrocyte Response*

The densities of GFAP-positive astrocytes of both halves under the moderate compression were significantly higher than those in sham animals ($p<0.001$ in the compressed half, $p<0.05$ in the contralateral half) (Fig. 8.3). The GFAP-positive glial density in the compressed half with moderate compression was significantly higher than seen with mild compression ($p<0.01$). Comparisons between the compressed and contralateral halves revealed that compressed half contained significantly higher GFAP-positive glial density than the contralateral half following either mild or moderate compression ($p<0.05$, $p<0.01$, respectively). As the compression increased, the density of GFAP-positive astrocytes increased markedly in the anterior horn of the compressed half (Fig. 8.4a).

In the dorsal horn, the density of the GFAP-positive glia of both halves with moderate compression was significantly higher than those in sham animals ($p<0.01$, $p<0.05$, respectively). Comparison of the two halves demonstrated no significant difference with mild compression; however, the glial density of the compressed half was significantly higher than that of the contralateral side under moderate compression ($p<0.01$) (Fig. 8.4b).

In the anterior funiculus, the GFAP-positive glial density in the two halves of the cord under mild and moderate compression was significantly higher than in the shams (each $p<0.01$). The glial density within the compressed half under the moderate compression was significantly higher than seen with mild compression ($p<0.01$). In contrast, the glial density within the contralateral half following moderate compression did not increase significantly compared to mild compression. Comparison of both halves of the spinal cord revealed no significant difference with mild compression; however, the glial density of the compressed half was markedly increased in comparison to the contralateral half following moderate compression ($p<0.05$) (Fig. 8.4c).

In the lateral funiculus, the GFAP-positive glial density within both halves of the spinal cord following mild and moderate compressions was significantly higher

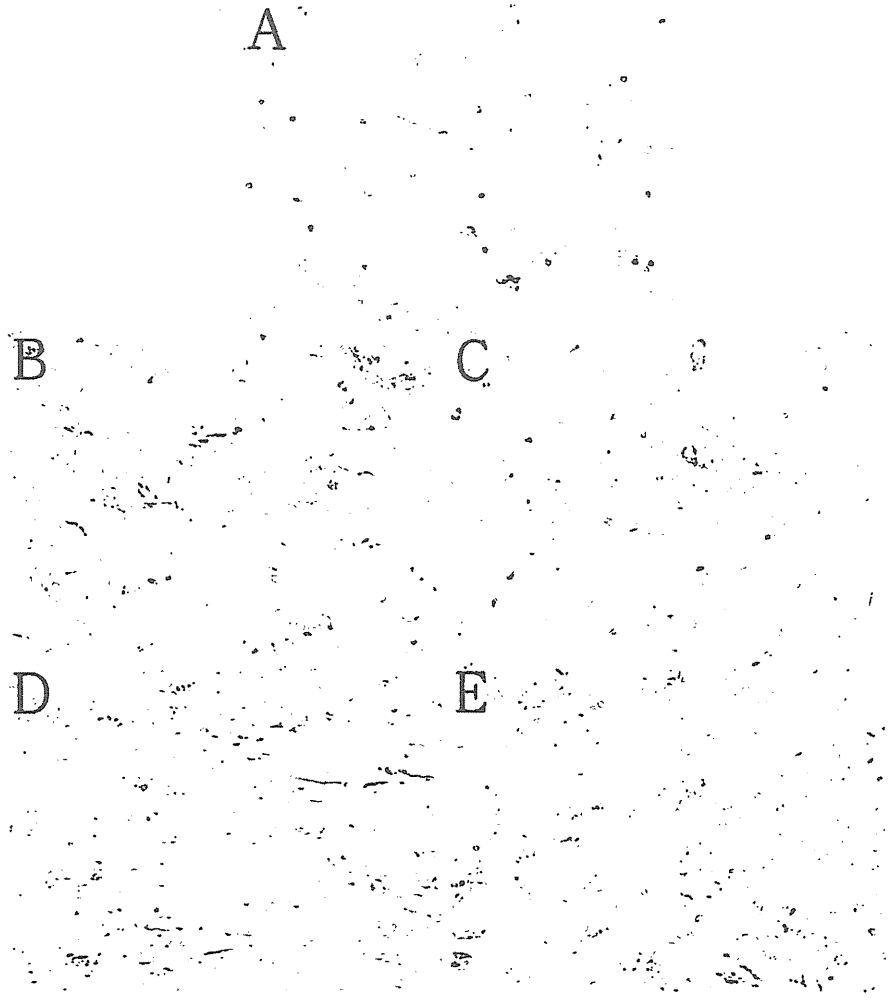

Fig. 8.3 Compared with the sham animals (a), extensive proliferation of GFAP-positive astrocytes in the anterior horn was seen in the compressed half (b) and the contralateral half (c) with mild compression and in the compressed half (d) and contralateral half (e) under moderate compression (GFAP stain, ×80)

than those in the sham animals (each $p<0.005$) (Fig. 8.5). Comparison of both halves of the spinal cord revealed no significant differences with the mild and moderate compression (Fig. 8.4d).

In the dorsal funiculus, the glial density in both halves under mild and moderate compression was significantly higher than in the shams (each $p<0.005$). There were no significant differences between either half of the cord following either mild or moderate compression (Fig. 8.4e).

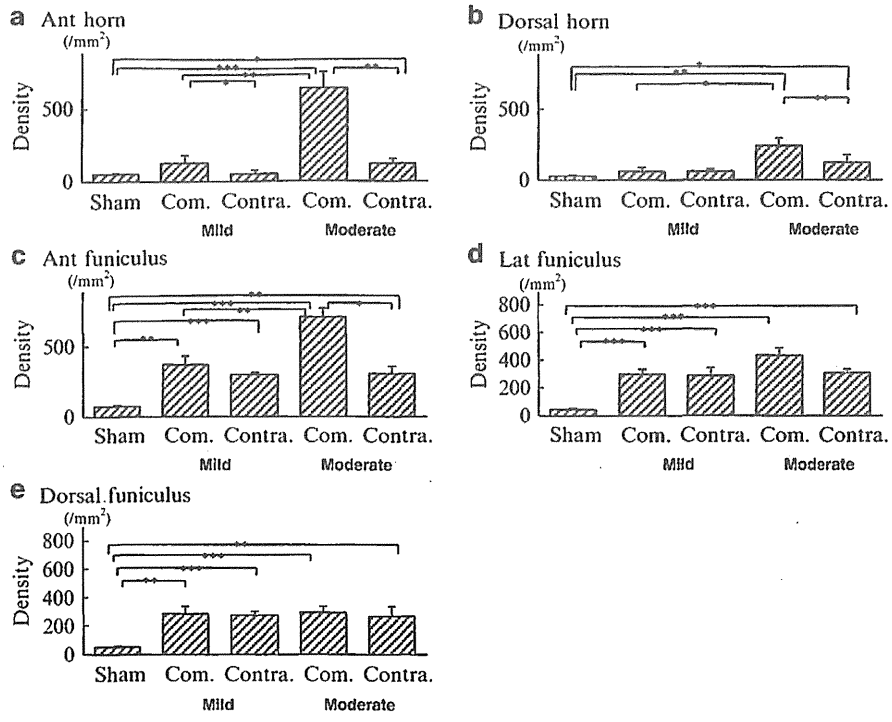

Fig. 8.4 The densities of GFAP-positive astrocytes increased in the two halves of the unilaterally compressed spinal cord. The density markedly increased in the *gray* matter and the anterior funiculus in the compressed half (Com.) compared with the contralateral half (Contra.) according to the increase in the compression. The differences in densities at the lateral and dorsal funiculi were not significant between the two halves of the spinal cord. (a) Anterior horn. (b) Dorsal horn. (c) Anterior funiculus. (d) Lateral funiculus. (e) Posterior funiculus (***$p<0.001$, **$p<0.01$, *$p<0.05$)

8.3.4 Relationship Between Area and Density of GFAP-Positive Astrocytes

The relationship between the area and the density of GFAP-positive astrocytes in the gray and white matter is shown in Fig. 8.6. Based upon the area reduction, the density of the compressed half increased more than that of the contralateral half in both the gray and white matter. Analyses of covariance (ANCOVA) were carried out to evaluate the influence of the compression on the variable density of GFAP-positive astrocytes in the gray and white matter independently of the area reduction. The densities of GFAP-positive astrocytes in the gray and white matter were entered as a dependent measure. The side of compressed or contralateral in the spinal cord

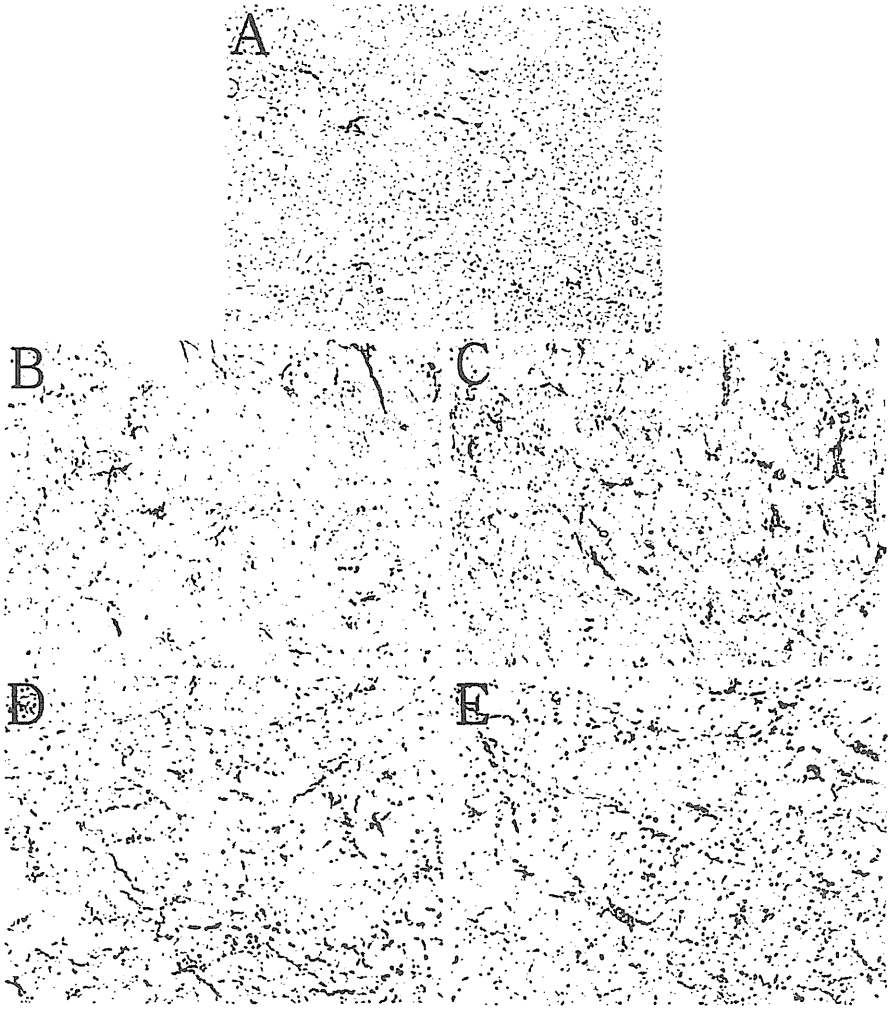

Fig. 8.5 Compared with the sham animals (a), extensive proliferations of GFAP-positive astrocytes at the lateral funiculus were seen in the compressed half (b) and the contralateral half (c) under mild compression and in the compressed half (d) and contralateral half (e) under moderate compression (GFAP stain, ×80)

was entered as a fixed variable, and the areas of gray and white matter were entered as covariate. The density of GFAP-positive astrocytes in the compressed half was significantly higher than that of the contralateral half in both the gray ($p<0.05$) and white matter ($p<0.05$). GFAP-positive astrocytes proliferated in the compressed half more than in the contralateral half of the unilaterally compressed spinal cord independent of the area reduction.

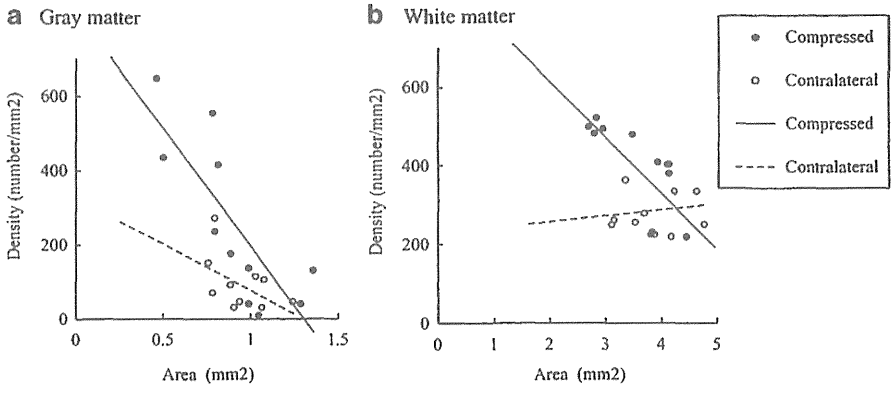

Fig. 8.6 Relationship between the area and the density of GFAP-positive astrocytes in the *gray* and *white* matter. Based on the area of reduction, the density of the compressed half increased more than that of the contralateral half in the gray and white matter. The density of GFAP-positive astrocytes in the compressed half was significantly higher than that of the contralateral half in the *gray* ($p<0.05$) and *white* matter ($p<0.05$) independently of the area reduction by ANCOVA. (a) *Gray* matter, (b) *white* matter

8.3.5 Microglia Response

Microglia were classified morphologically into resting and reactive microglia based on the RCA-1-positive structures observed by a light microscopy. The resting microglia have long finely branched processes from mainly opposite poles of the perinuclear cytoplasm. The reactive microglia have shortened and thickened processes that extend in all directions from enlarged cytoplasms.

In the sham group, resting microglia with long finely branched processes from perinuclear cytoplasms were observed adjacent to neurons in the gray matter more than in the white matter in the lectin RCA-1 immunostaining. No reactive microglia was found in both gray and white matters.

In the mild compression group, the mild proliferation of reactive microglia, which have shortened and thickened processes that extend in all directions from enlarged cytoplasms, was observed in the anterior horn of the compressed half of the spinal cord. In contrast, only a few reactive microglia were observed in the anterior horn of the contralateral half. No reactive microglia was found in the white matters on both halves (Fig. 8.7).

The numbers of resting and reactive microglia in the sham and mild compression groups are shown in Table 8.2. There was no significant difference in the total numbers of resting and reactive microglia in the gray and the white matters between the sham and mild compression groups 48 h after the surgery. Reactive microglia in the anterior horn of the compressed half, however, increased significantly compared to the other areas and it was not observed in the white matter.

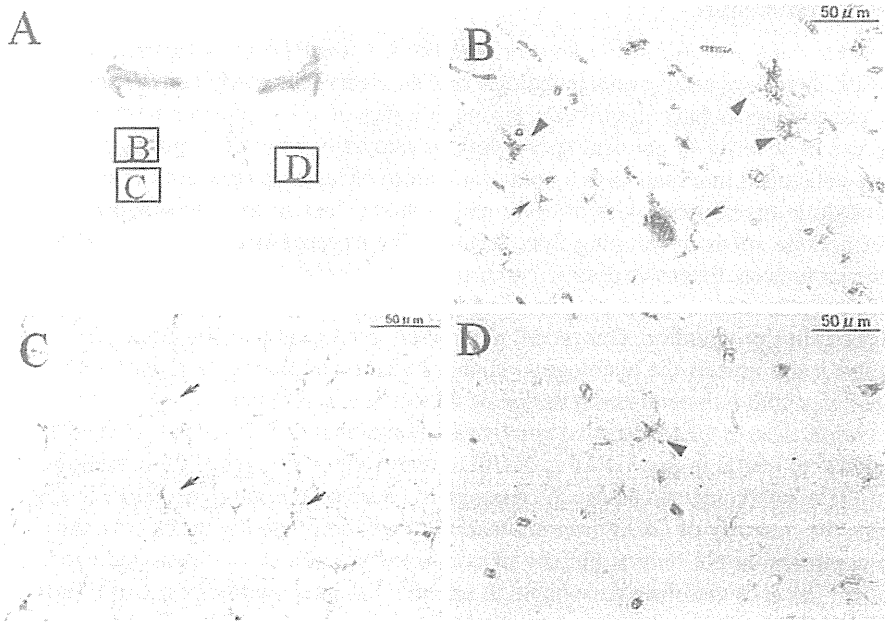

Fig. 8.7 In the deformed spinal cord under mild compression (**a**), reactive microglias (*arrowhead*) and resting microglias (*arrow*) were observed in the anterior horn of the compressed half (**b**). *Asterisks* show some of RCA-positive vascular vessels. No reactive microglia was found in the white matter of the compressed half (**c**). A few reactive microglias (*arrowhead*) were observed in the anterior horn of the contralateral half (**d**) (RCA-1 stain, ×200)

Table 8.2 The numbers of resting and reactive microglia in the mild compression and sham groups (mean ± SD)

		Mild compression			Sham[a]
		Resting	Reactive	Total	Resting
Compression side (right side)	Anterior horn	18.8±5.9	10.8±3.3[b]	29.6±3.3	31.0±2.8
	Dorsal horn	25.2±4.9	3.8±3.8	29.0±1.9	32.5±3.5
	Anterior funiculus	14.6±0.5	0±0	14.6±0.5	17.5±0.7
	Lateral funiculus	14.8±0.8	0±0	14.8±0.8	16.0±1.4
	Dorsal funiculus	15.8±2.0	0±0	15.8±2.0	14.5±0.7
Contralateral side (left side)	Anterior horn	26.8±4.8	2.6±2.2	29.4±3.1	31.0±4.2
	Dorsal horn	29.2±2.0	0.2±0.4	29.4±2.1	29.5±0.7
	Anterior funiculus	14.8±1.3	0±0	14.8±1.3	17.0±1.4
	Lateral funiculus	16.6±1.8	0±0	16.6±1.8	16.6±0.0
	Dorsal funiculus	15.8±1.1	0±0	15.8±1.1	16.0±1.4

[a]No reactive microglia was found in any area in the sham group
[b]Significantly higher than the dorsal horn of the compression side and anterior and dorsal horn of contralateral side ($p<0.01$)

8.4 Discussion

To date, there have been several pathologic studies of cervical spondylotic myelopathy. Ito and colleagues have described neuropathologies of seven patients with various degrees of severity of cervical spondylotic myelopathy who were autopsied [14]. They concluded that there was a common pattern of lesion progression in cervical spondylotic myelopathy with atrophy and neuronal loss in the anterior horn and intermediate zones developing first, followed by degeneration of the lateral and posterior funiculi. Extensive destructive change such as axonal loss, myelin destruction, and cavity formation in the degenerating spinal cord was observed in the terminal stages of this progression. Our model most likely corresponds to the latent stage of paralysis and reveals the histological changes that are associated with myelopathy in patients with unilateral compression of the cervical spinal cord.

Proliferation of GFAP-positive astrocytes is considered as the hallmark of the CNS response to neural injury. GFAP is useful to detect the gliotic response in ischemic brain injury [15, 16] and assess the damage in neurotoxic brain injury [17]. In this study, the intensity of GFAP immunoreactivity was correlated with the severity of the compression not only at the site of compression but also at rostral and caudal points [18]. It is therefore reasonable to assume that increased numbers of GFAP-positive astrocytes can serve as an indicator of tissue injury in CNS. This assumption, however, must be evaluated in relation to any potential reduction in the issue area. The results of ANCOVA performed to evaluate the GFAP-positive astrocyte proliferation independent of the area reduction clearly demonstrated that GFAP-positive astrocytes proliferated in the compressed half more than in the contralateral half of the unilateral compressed spinal cord.

Microglias, one of the inflammatory cells in the CNS, are rapidly activated in response to any CNS insult. Microglial activation occurs as a graded response, characterized by their transformation into phagocytic cells with macrophage-like morphology (reactive microglia) and proliferation [19]. In the present study, the distribution of GFAP-positive astrocytes in the unilateral spinal compression corresponded to that of reactive microglia. Microglia respond more rapidly than any other cells to a variety of injuries in the CNS [20]. The microglial reaction precedes the astroglial reaction by release of astroglia-stimulating factors [21] and macrophage migration inhibitory factor [22], which increase astrocytic glutamine synthetase and GFAP immunoreactivity and promote reactive astrocytosis. These studies account for the analogy between the distributions of the reactive microglia and the GFAP-positive astrocytes in the present study.

In the present study, damage occurred even in the contralateral half of the unilaterally compressed spinal cord due to the mechanical stress exerted from the compressed half of the spinal cord. Using a finite element analysis model (FEM) of unilateral spinal cord compression, the stress concentration at the gray matter of the compressed half was markedly higher than that of the contralateral half. In contrast, equivalent stress concentrations were shown in the lateral funiculus of both halves [23]. The density of GFAP-positive astrocytes reported in the present

study was compatible with the stress distributions predicted from the FEM. The observed discrepancy in the histological reaction between the anterior horn and the lateral funiculus of the two halves is most likely linked to differences in the stress concentration.

In compression myelopathy, neurological symptoms and signs theoretically depend on the site and severity of the compression. The compression of only a half of the spinal cord should present a pure Brown-Séquard syndrome. However, only 23 % of 129 paramedian herniation cases with cervical myelopathy presented Brown-Séquard syndrome, whereas the remaining 77 % presented transverse lesion syndrome. The majority of patients with transverse lesion syndrome revealed the ipsilateral predominant palsy of the same upper limb as the compressed side of the spinal cord and bilateral motor and sensory deficits of the lower limbs that were equivalent [7]. Based on the density of GFAP-positive astrocytes in the unilateral compressed spinal cord, the damage in the gray matter of the compressed half was significantly higher than that of the contralateral half, whereas the damage at the lateral funiculus, where the lateral pyramidal and the dorsal spinocerebellar tracts are located, and the dorsal funiculus did not show significant differences between the compressed and contralateral halves. These findings provide evidence for the mechanistic basis of spinal cord damage that leads to transverse lesion syndrome in unilateral compression myelopathy.

8.5 Conclusion

Under the unilateral compression, the density of GFAP-positive astrocytes in the gray matter and the anterior funiculus increased significantly in the compressed half compared to the contralateral half of the spinal cord. The densities in the lateral and dorsal funiculi, however, were not significant differences between the both halves. The distribution of GFAP-positive astrocytes in the unilateral spinal compression corresponded to that of reactive microglia. These findings provide evidence for the mechanistic basis by which unilateral compression induces transverse damage to the spinal cord.

Conflict of Interest The authors declare that they have no conflict of interest.

References

1. Brain W, Northfield D, Wilkinson M (1952) The neurological manifestations of cervical spondylosis. Brain 75:187–225
2. Hinck VC, Sachdev NS (1966) Developmental stenosis of the cervical spinal canal. Brain 89:27–36
3. Fujiwara K, Yonenobu K, Ebara S et al (1989) The prognosis of surgery for cervical compression myelopathy. An analysis of the factors involved. J Bone Joint Surg Br 71:393–398
4. Crandall PH, Batzdorf U (1966) Cervical spondylotic myelopathy. J Neurosurg 25:57–66

5. Jabbari B, Pierce JF, Boston S et al (1977) Brown-Séquard syndrome and cervical spondylosis. J Neurosurg 47:556–560
6. Finelli PF, Leopold N, Tarras S (1992) Brown-Séquard syndrome and herniated cervical disc. Spine 17:598–600
7. Kokubun S, Tanaka Y (1995) Type of cervical disc herniation and relation to myelopathy and radiculopathy. J Back Musculoskelet Rehabil 5:145–154
8. Hashizume Y, Iijima S, Kishimoto H et al (1984) Pathology of spinal cord lesions caused by ossification of the posterior longitudinal ligament. Acta Neuropathol (Berl) 63:123–130
9. Harkey HL, Al-Mefty O, Marawi I et al (1995) Experimental chronic compressive cervical myelopathy: effects of decompression. J Neurosurg 83:336–341
10. Uchida K, Baba H, Maezawa Y et al (1998) Histological investigation of spinal cord lesions in the spinal hyperostotic mouse (twy/twy): morphological changes in anterior horn cells and immunoreactivity to neurotropic factors. J Neurol 245:781–793
11. Ozawa H, Wu ZJ, Tanaka Y et al (2004) Morphologic change and astrocyte response to unilateral spinal cord compression in rabbits. J Neurotrauma 21:944–955
12. Tarlov I, Klinger H (1954) Spinal cord compression studies 2. Time limits for recovery after acute compression in dogs. AMA Arch Neurol Psych 71:271–290
13. He BP, Strong MJ (2000) A morphological analysis of the motor neuron degeneration and microglial reaction in acute and chronic in vivo aluminum chloride neurotoxicity. J Chem Neuroanat 17:207–215
14. Ito T, Oyanagi K, Takahashi H et al (1996) Cervical spondylotic myelopathy. Clinicopathologic study on the progression pattern and thin myelinated fibers of the lesions of seven patients examined during complete autopsy. Spine 21:827–833
15. Schmidt-Kastner R, Szymas J, Hossmann KA (1990) Immunohistochemical study of glial reaction and serum-protein extravasation in relation to neuronal damage in rat hippocampus after ischemia. Neuroscience 38:527–540
16. Norenberg MD (1994) Astrocyte responses to CNS injury. J Neuropathol Exp Neurol 53:213–220
17. O'callaghan JP (1991) Assessment of neurotoxicity: use of glial fibrillary acidic protein as a biomarker. Biomed Environ Sci 4:197–206
18. Farooque M, Badonic T, Olsson Y et al (1995) Astrocytic reaction after graded spinal cord compression in rats: immunohistochemical studies on glial fibrillary acidic protein and vimentin. J Neurotrauma 12:41–52
19. Kreutzberg GW (1996) Microglia: a sensor for pathological events in the CNS. Trends Neurosci 19:312–318
20. Gehrmann J, Matsumoto Y, Kreutzberg GW (1995) Microglia: intrinsic immuneffector cell of the brain. Brain Res Brain Res Rev 20:269–287
21. Giulian D, Young DG (1986) Brain peptides and glial growth II. Identification of cells that secrete glia-promoting factors. J Cell Biol 102:812–820
22. Koda M, Nishio Y, Hashimoto M et al (2004) Up-regulation of macrophage migration-inhibitory factor expression after compression-induced spinal cord injury in rats. Acta Neuropathol 108:31–36
23. Ozawa H, Kokubun S, Ohashi T et al (2002) Biological and biomechanical analysis of the response to unilateral spinal cord compression. J Jpn Orthop Assoc 76:S940 (In Japanese)

Chapter 25
Stress Distribution of the Spinal Cord and Clinical Relevance in Cervical Spondylotic Myelopathy

Kohei Takahashi, Hiroshi Ozawa, Naoya Sakamoto, Yuka Minegishi, Masaaki Sato, and Eiji Itoi

Abstract Intramedullary stress was analyzed in patients with cervical spondylotic myelopathy (CSM) using a finite element method (FEM). A total of 99 disc levels of 30 patients with CSM were analyzed and divided into two groups: 33 disc levels with high signal intensity (HSI) on T2WI MRI (HSI group) and 66 disc levels without HSI (non-HSI group). Ninety disc levels of 30 patients without myelopathy were set up as a control group. The stress in the HSI group was significantly highest among three groups. The cutoff value to present HSI was 2.30 kPa from a receiver operator characteristics (ROC) analysis. A multiple logistic regression analysis was performed to compare the utility of the three parameters as prognosticators for the onset of myelopathy: intramedullary stress, the cross-sectional area of the spinal

K. Takahashi
Department of Orthopaedic Surgery, Tohoku University School of Medicine,
1-1 Seiryomachi, Aobaku, Sendai 980-8574, Japan

Department of Orthopaedic Surgery, Senboku Kumiai Hospital,
1-30 Toricho Omagari, Daisen, Akita 014-0027, Japan

H. Ozawa (✉) • E. Itoi
Department of Orthopaedic Surgery, Tohoku University School of Medicine,
1-1 Seiryomachi, Aobaku, Sendai 980-8574, Japan
e-mail: hozawa@med.tohoku.ac.jp

N. Sakamoto
Graduate School of Biomedical Engineering, Tohoku University,
6-6-04 Aramaki Aoba, Aobaku, Sendai 980-8578, Japan

Department of Medical Engineering, Kawasaki University of Medical Welfare,
288 Matsushima, Kurashiki, Okayama 701-0193, Japan

Y. Minegishi • M. Sato
Graduate School of Biomedical Engineering, Tohoku University,
6-6-04 Aramaki Aoba, Aobaku, Sendai 980-8578, Japan

K. Uchida et al. (eds.), *Neuroprotection and Regeneration of the Spinal Cord*,
DOI 10.1007/978-4-431-54502-6_25, © Springer Japan 2014

cord, and the anteroposterior compression ratio (APCR). Intramedullary stress had the highest odds ratio. The intramedullary stress significantly reduced after surgery. From the analysis of the correlation between the local kyphosis angle and the reduction of the stress after surgery in HSI group, the higher the kyphosis was, the less the reduction of the stress after surgery. In conclusion, intramedullary stress reflected clinical manifestations in patients with CSM.

Keywords Cervical spondylotic myelopathy • Finite element method • Intramedullary stress

25.1 Introduction

In patients with cervical spondylotic myelopathy (CSM), symptoms are attributed to compression of the spinal cord. However, compression of the spinal cord does not always induce symptomatic myelopathy. It is observed in 7.6–26 % of asymptomatic subjects [1, 2].

Numerous factors that contribute to the onset of cervical myelopathy have been reported. However, the degree of spinal cord compression inducing myelopathy remains inadequately understood. The cross-sectional area of the spinal cord and the anteroposterior compression ratio (APCR) of the spinal cord have been reported to be factors indicating the relationship between spinal cord deformities and symptoms of CSM [3–6]. However, it is not easy to evaluate whether the compression is symptomatic in the clinical practice even with those parameters.

Ozawa et al. [7] reported that the distribution of pathological changes in a unilateral spinal cord compression model using rabbits is compatible with the stress distribution drawn from the finite element method (FEM) model. Also, there have been several reports that show the significance of intramedullary stress to the pathogenesis of CSM by biomechanical simulations of cervical spinal cord compression using FEM [8–10]. However, there has been no research that clinically examines the relationship between neurological condition and intramedullary stress distribution in actual patients with CSM.

We considered that intramedullary stress is strongly related to the pathogenesis of cervical myelopathy. To clarify the influence of intramedullary stress on CSM, intramedullary stress distribution of the spinal cord was analyzed in patients with CSM using the FEM, and then the following four issues were investigated.

1. Influence of intramedullary stress on the onset of CSM
2. Comparison of clinical relevance among intramedullary stress, cross-sectional area, and APCR
3. Change of the intramedullary stress after decompression surgery
4. Relationship of intramedullary stress to sagittal alignment of cervical spine

25.2 Material and Methods

25.2.1 Creating an FEM Model to Analyze Intramedullary Stress

25.2.1.1 Extracting the Shape of the Spinal Cord

A midsagittal image of T2-weighted magnetic resonance image (T2WI) of the cervical spine was scaled up five times on a tablet (Cintiq 12WX®, Wacom, Japan). The anterior and posterior margins of the spinal cord from the inferior margin of the vertebral body of C2 to the inferior margin of the vertebral body of C7 were marked manually with dots at intervals of approximately 1 mm. The coordinate data of these dots were obtained using ImageJ® software (National Institutes of Health, NIH) (Fig. 25.1). The anterior and posterior margins were approximated by spline curves made from the coordinate data. The shape of the spinal cord was determined by combining the spline curves of the anterior and posterior margins.

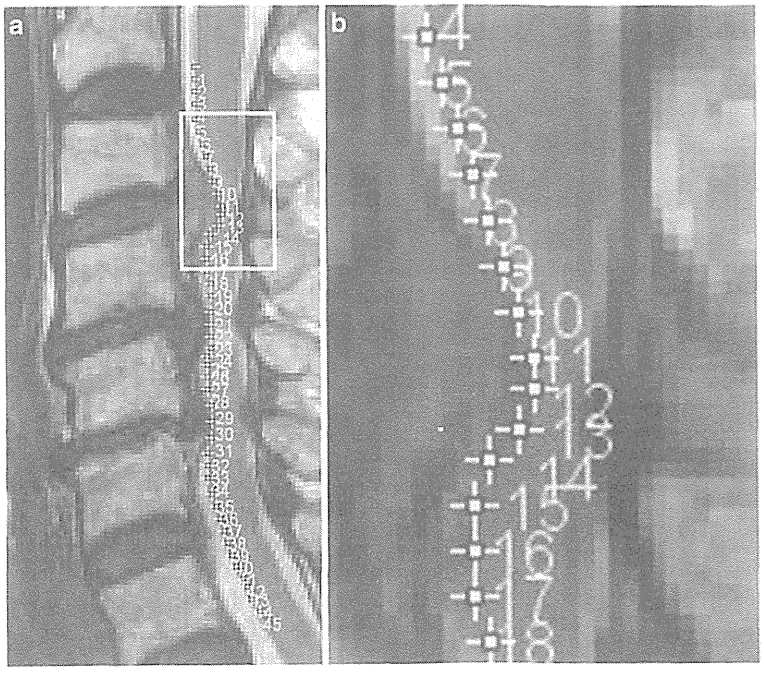

Fig. 25.1 Extracting the shape of the spinal cord. On the midsagittal T2WI images of the cervical spine, the anterior and posterior margins of the spinal cord from the inferior margin of the vertebral body of C2 to the inferior margin of the vertebral body of C7 were marked with dots at intervals of approximately 1 mm (**a**). (**b**) is a magnified figure of the square in (**a**)

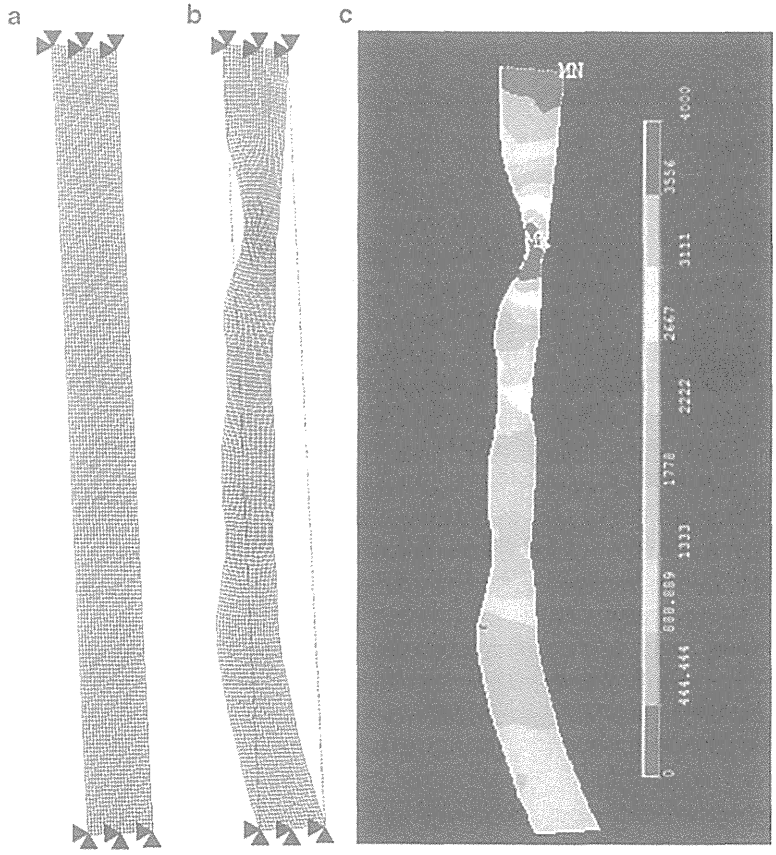

Fig. 25.2 FEM analysis. A straight line model was made by connecting the cranial and caudal corners of the spinal cord approximated by the spline curves (**a**). Then, the fixed displacement obtained from the spinal cord shape was imposed on the straight line model (**b**) and the stress distribution was quantified as the von Mises equivalent stress (**c**)

25.2.1.2 FEM Analysis

A straight line model made by connecting the cranial and caudal corners of the spinal cord approximated by the spline curves was constructed with 4,000 two-dimensional eight-node elements (Fig. 25.2a). Both the cranial (top) and caudal (bottom) edges of the model were constrained in all directions. Then, the fixed displacement obtained from the spinal cord shape was imposed on the straight line model (Fig. 25.2b) and the stress distribution was quantified as the von Mises equivalent stress using Ansys 11.0 software (Ansys Ver. 11, Ansys Inc., USA) (Fig. 25.2c). The initial modulus of elasticity and Poisson's ratio of the spinal cord were applied as 5 kPa and 0.49, respectively, based on a previous study [11]. The area from the middle of the vertebral body of C3 to the middle of the vertebral body of C4 was defined as the C3–4 disc level. The C4–5 and C5–6 disc levels were similarly defined (Fig. 25.3). The maximum stress value at each disc level was defined as the stress at that segment.

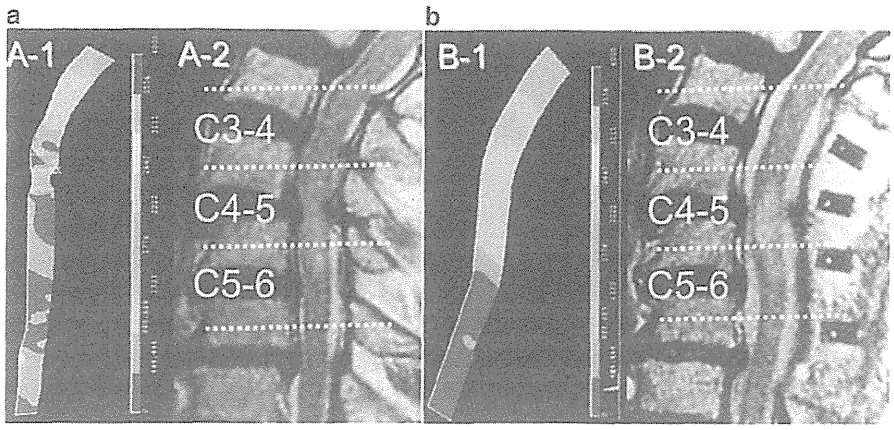

Fig. 25.3 On the preoperative midsagittal T2WI image, the intramedullary stress distribution was analyzed (a). The C4-5 disc level presented the highest stress. The postoperative stress was analyzed from midsagittal T2WI image (b). The stress at the C4-5 disc level reduced markedly

25.2.2 Patients for Analysis

Thirty-three consecutive patients (21 males and 12 females) with CSM who underwent Kurokawa's laminoplasty at one hospital were evaluated. These patients had been participants of another study designed as a prospective study [12]. All patients with CSM clinically presented transverse lesion syndrome consisting of bilateral motor and sensory deficits of the upper and lower limbs with exaggerated knee and Achilles jerks. These patients underwent preoperative MRI and then postoperative MRI 4 weeks after surgery. The mean age of the patients was 62.1 ± 11.0 (mean±SD) years (95 % confidence interval: 58.2–66.0).

All patients presented high signal intensity (HSI) in any of three disc levels of C3–4, C4–5, and C5–6 on T2WI MRI. The disc levels with HSI were at C3–4 in six cases, at C4–5 in 13 cases, and at C5–6 in 14 cases. A total of 99 disc levels from C3 to C6 in 33 patients were divided into two groups: 33 disc levels with HSI (HSI group) and 66 disc levels without HSI (non-HSI group).

Thirty patients (18 males and 12 females) who underwent cervical MRI for reasons other than myelopathy were enrolled in this study, and 90 disc levels from C3 to C6 were set up as a control group. The mean age of the control patients was 62.1 ± 13.0 (mean±SD) (95 % confidence interval: 57.3–66.9) years. All patients with CSM had spinal cord compression at least in one disc level and some of them had multilevel compression on MRI, while patients in the control group had no obvious spinal cord compression. None of the disc levels in the control group presented HSI on T2WI.

25.3 Illustrative Case

The patient was an 82-year-old male. The disc level presenting HSI was C4–5. The highest intramedullary stress was demonstrated in C4–5 disc level (C3–4: 1.7 kPa, C4–5: 2.9 kPa, and C5–6: 0.7 kPa) (Fig. 25.3a). The intramedullary stress at each disc level was clearly reduced after posterior decompression surgery (C3–4: 1.3 kPa, C4–5: 1.0 kPa, and C5–6: 0.5 kPa) (Fig. 25.3b).

25.4 Influence of Intramedullary Stress on the Onset of Cervical Spondylotic Myelopathy

25.4.1 Relationship Between HSI and Intramedullary Stress

To evaluate the relationship between intramedullary stress and spinal cord degeneration, intramedullary stress was compared among the HSI group, the non-HSI group, and the control group. In all patients with CSM, the disc level with HSI presented the highest stress among the three disc levels evaluated. Intramedullary stress was 3.16±0.86 kPa (mean±SD) in the HSI group, 1.81±0.72 kPa in the non-HSI group, and 1.01±0.37 kPa in the control group. The stress in the disc level with HSI was significantly highest among three groups ($p<0.0001$) (Fig. 25.4).

Intramedullary signal change on MRI is generally considered to reflect nerve tissue degeneration [13]. In addition, the level of HSI on T2WI was deemed responsible for symptoms [14, 15]. In the present study, HSI was strongly associated with intramedullary stress. Thus intramedullary high stress due to spinal cord compression was considered to induce nerve tissue damage, resulting in the onset of CSM.

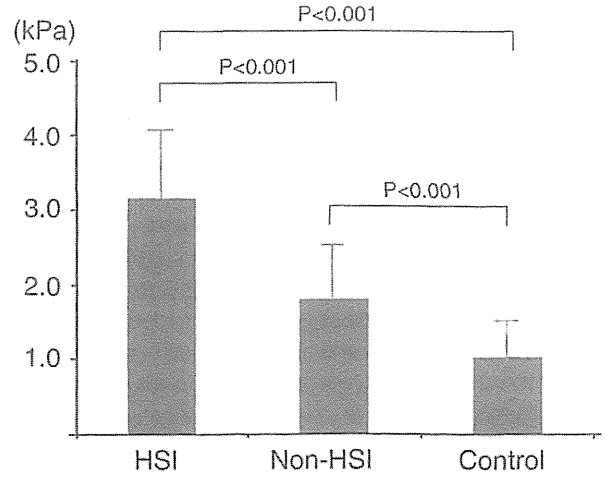

Fig. 25.4 The stress in the HSI group was significantly largest among three groups

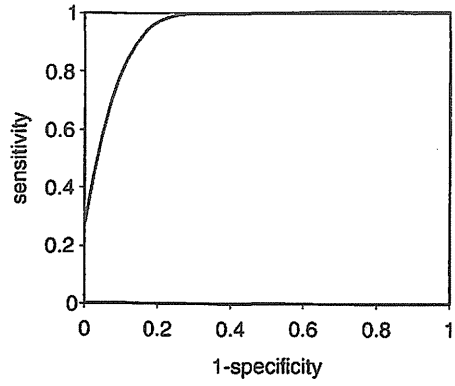

Fig. 25.5 Receiver operator characteristics curve for intramedullary stress. The areas under the curve (AUC) was 0.95. The most qualified cutoff value to cause the HSI was 2.30 kPa (sensitivity 78.8 %, specificity 91.9 %)

25.4.2 Cutoff Value of Stress to Induce HSI

The cutoff value of stress to induce HSI was investigated. A total of 189 disc levels in three groups were analyzed from a receiver operator characteristics (ROC) curve, and the cutoff value of stress to present HSI was investigated. The ROC curve is shown in Fig. 25.5. The area under the curve (AUC) was 0.95. The qualified cutoff value to cause the HSI was 2.30 kPa (sensitivity 78.8 %, specificity 91.9 %). There was no disc level presenting high intramedullary stress over 2.3 kPa without spinal cord compression on MRI. None of the disc levels in the control group exceeded 2.30 kPa.

Compression of the spinal cord is observed in 7.6–26 % of asymptomatic subjects [1, 2]. It is not easy to evaluate whether compression of the spinal cord is symptomatic. No disc level in the control group exceeded the cutoff value which was presented in the present study. We considered, therefore, that a threshold of intramedullary stress to present symptoms of myelopathy actually existed. That is, when the intramedullary stress reaches at some extent, neurological dysfunction should become obvious.

25.5 Comparison of Clinical Relevance Among Intramedullary Stress, Cross-Sectional Area, and APCR

A multiple logistic regression analysis was performed to compare the utility of each of these three parameters as prognosticators for the onset of myelopathy. The objective variable was whether the segment presented HSI, while the explanatory variables were stress, cross-sectional area, and APCR. The cutoff values for all the explanatory variables were obtained from the ROC analysis, and explanatory variables were converted to two-valued variables based on the cutoff values. The cutoff values for cross-sectional area and APCR were 57.3 mm^2 (sensitivity 69.7 %, specificity 69.7 %) and 36.2 % (sensitivity 75.8 %, specificity 74.3 %), respectively. The result of the multiple logistic regression analysis was shown in Table 25.1. The odds ratios for stress, cross-sectional area, and APCR were 11.1, 4.1, and 4.3, respectively. Stress showed

Table 25.1 Odds ratio of prognostic parameters

	Odds ratio (95 % CI)	*P* value
Intramedullary stress	11.1 (3.67–38.6)	$p<0.0001$
Area of spinal cord	4.1 (1.30–13.8)	$p=0.016$
APCR	4.3 (1.4–14.1)	$p=0.011$

APCR anteroposterior compression ratio

the largest odds ratio and was found to be the most useful prognosticator for the onset of myelopathy.

In the present study, the disc level with HSI presented the highest stress and the smallest cross-sectional area of the spinal cord among the three disc levels evaluated in all cases. However, in three cases, the disc levels with HSI did not correspond to the disc levels of the lowest APCR. The APCR does not express the severity of spinal cord deformities in some cases, for example, in cases in which the spinal cord is deformed into a boomerang shape or comma shape. We believe that the APCR is not an adequate parameter to express spinal cord deformities since it is calculated only for the transverse and anteroposterior diameters.

Penning et al. [6] reported that long tract signs appear when the cross-sectional area of the spinal cord is reduced by approximately 60 mm^2 or less, based on an analysis of CT myelograms in 80 cases of CSM. Kadanka et al. [5] reported that a cross-sectional area of the spinal cord between 50 and 60 mm^2 is the critical value for significant disability, based on a prospective study of a large cohort of patients with CSM. On the other hand, Golash et al. [16] suggested that the cross-sectional area of the spinal cord is not a prognosticator for the presence of myelopathy since the area overlaps significantly between patients with and those without myelopathy. Kato et al. [17] reported that the cross-sectional area of the spinal cord at any disc level shows a dispersion with a standard deviation of approximately 10 mm^2 based on the cervical MRI images of 1,211 asymptomatic subjects. The absolute value of the cross-sectional area of the spinal cord does not predict the onset of CSM.

We analyzed the intramedullary stress of the patients with CSM from sagittal image. A stress analysis of sagittal MR images reflects both the spinal cord compression and sagittal alignment of the spinal cord, which cannot be expressed on axial images. The sagittal alignment of the cervical spine has a potent effect on the prognosis of CSM [18]. The method of analysis of the sagittal plane implemented in the present study was considered to have an advantage for investigating the pathological conditions of the spinal cord.

25.6 Preoperative and Postoperative Stress Values of the HSI Group

Preoperative and postoperative stress values of the HSI group were compared using paired t-test. The preoperative stress in the HSI group was 3.16 ± 0.86 kPa, and the postoperative stress was down to 1.38 ± 0.43 kPa. It reduced significantly after the surgery ($p<0.0001$) (Fig. 25.6).